Mathematical and Computational Applications

MDPI

Article

Role of Nanoparticles and Heat Source/Sink on MHD Flow of Cu-H_2O Nanofluid Flow Past a Vertical Plate with Soret and Dufour Effects

Ramesh Kune [1], Hari Singh Naik [2], Borra Shashidar Reddy [1] and Christophe Chesneau [3,*]

1 Sreenidhi Institute of Science and Technology, Ghatkesar, Hyderabad 501301, India
2 Department of Mathematics, Osmania University, Hyderabad 500007, India
3 Department of Mathematics, University of Caen-Normandy, 14000 Caen, France
* Correspondence: christophe.chesneau@unicaen.fr

Abstract: The study is devoted to investigating the effect of an unsteady non-Newtonian Casson fluid over a vertical plate. A mathematical analysis is presented for a Casson fluid by taking into consideration Soret and Dufour effects, heat generation, heat radiation, and chemical reaction. The novelty of the problem is the physical interpretation of Casson fluid before and after adding copper water-based nanoparticles to the governing flow. It is found that velocity was decreased and the temperature profile was enhanced. A similarity transformation is used to convert the linked partial differential equations that control flow into non-linear coupled ordinary differential equations. The momentum, energy, and concentration formulations are cracked by means of the finite element method. The thermal and solute layer thickness growth is due to the nanoparticles' thermo-diffusion. The effects of relevant parameters such as the Casson fluid parameter, radiation, Soret and Dufour effects, chemical reaction, and Prandtl number are discussed. A correlation of the average Nusselt number and Sherwood number corresponding to active parameters is presented. It can be noticed that increasing the Dufour number leads to an uplift in heat transfer. Fluid velocity increases with Grashof number and decreases with magnetic effect. The impact of heat sources and radiation is to increase the thermal conductivity. Concentration decreases with the Schmidt number.

Keywords: Casson nanofluid; copper nanoparticle; Soret and Dufour effects; chemical reaction

Citation: Kune, R.; Naik, H.S.; Reddy, B.S.; Chesneau, C. Role of Nanoparticles and Heat Source/Sink on MHD Flow of Cu-H_2O Nanofluid Flow Past a Vertical Plate with Soret and Dufour Effects. *Math. Comput. Appl.* **2022**, *27*, 102. https://doi.org/10.3390/mca27060102

Academic Editors: Gianluigi Rozza and Sivasankaran Sivanandam

Received: 29 September 2022
Accepted: 24 November 2022
Published: 28 November 2022

1. Introduction

Nanoparticles and nanofluid are both terms for particles with a diameter of less than one nanometer. Choi [1] is credited with creating the phrase "nanofluid". Inorganic compounds typically make up nanoparticles. Compared to conventional heat transfer fluids, nanofluids exhibit finer heat transfer characteristics. The idea of a nanofluid has been put forth as a means of improving heat-transfer liquid performance significantly. There is a good deal of research on convective heat transport in nanofluids and issues related to stretching surfaces, since nanofluids are becoming more important. Himanshu et al. [2] reported the magnetohydrodynamics of Ag-water nanofluid over a stretching flat plate in a porous medium. Mishra et al. [3] unveiled the combined effect of pertinent parameters on the MHD flow of Ag-H_2O nanofluid into a porous stretching/shrinking channel. Stagnation point flows of upper convex Maxwell fluid past a stretching plate are evaluated by Ibrahim and Negera [4]. In their valuable work, Kataria et al. [5] originated the concept of heat generation/absorption magnetohydrodynamic via fluid flow past a porous vertical plate. The problem is solved by employing the Laplace transform technique, and the physical significance of pertinent parameters is tested. Kumar et al. [6] analyzed the performance of Casson and Maxwell fluids past a stretching sheet with an internal heat source and sink. It was reported that the thermal and concentration fields of Maxwell fluid are highly influenced by the non-dimensional parameters, compared to Casson fluid. Swain et al. [7]

surveyed the incompressible Newtonian fluid over a porous stretching sheet. The impact of the porous parameter acting as an aiding force is reported in this study. Muhammed et al. [8] analyzed the 3D stretched flow of viscous dissipation with prescribed heat and concentration fluxes. In this research study, a withal magnetic field is applied in the flow region, and mathematical equations with physical quantifiers are formulated. Jithender et al. [9] demonstrated unsteady MHD Casson flow for the geometrical model of a plate in oscillation motion vertically, and the numerical outputs were obtained by computing the finite element method. Basant et al. [10] used two concentric cylinders to model a vertical annular micro-channel under the influence of a radial magnetic field. Amira et al. [11] improved the idea of hybrid nanofluids expressing mathematical models of stretching and shrinking sheets, and flow equations were solved by means of appropriate similarity transformations. Jawad et al. [12] investigated heat transfer in a semi-porous channel with stretching walls using MHD nanofluids. The channel was filled with an incompressible copper–water nanofluid and the outputs were revealed graphically. Gireesha et al. [13] examined the rate of nanoparticle injection and chemical reaction from steady planar Couette flow through a permeable micro-channel using the Runge–Kutta–Fehlberg fourth order. Recently, an increasing number of studies concerning nanofluids have been described in [14–18]. The impression of Soret and Dufour effects boosts the transmission of heat and mass. These effects play an important role when there are density differences in the flow. Hayat et al. [19] generalized three-dimensional radiative flow with Soret and Dufour effects. Saritha et al. [20] analyzed Soret and Dufour combined impact on the MHD flow of a power-law fluid across a flat plate. On a flat plate, MHD boundary-layer slip flow with Soret and Dufour implications was reported by Reddy and Saritha [21]. The investigation flow model is filled with second grade fluid, electrically conducting through a magnetic field. Jyotsa et al. [22] have identified an advanced mathematical model of exponentially accelerated inclined plates and dimensionless quantifiers that are tested for radiation and magnetic strength. [23]. Rashidi et al. [24] conveyed a buoyancy effect on the MHD flow of nanofluid over a stretching sheet. Studies on how different MHD nanofluids transmit heat differently due to differences in shape were carried out by [25–28].

Anil Kumar et al. [29] studied how a transient convective nanofluid that streams along a vertical plate is affected by radiation and magnetic fields. In the literature on studies of nanofluids, the impact of Soret–Dufour is mostly neglected. Casson fluid is a shear-thinning fluid, that is assumed to have an infinite viscosity at zero rate of shear. Chang et al. [30] investigated the rheology of CuO nanoparticles. This study aims to compare Casson and Casson nanofluid and to investigate the chemical effects of Soret and Dufour on the fluid domain surface.

2. Problem Formulation

We will now explain the physical problem at hand by assuming an unsteady viscous nanofluid flowing through a suddenly initiated vertical plate. The coordinate model is chosen [31,32] so that the x and y axes are parallel and normal to the plate, respectively. The plate and the nanofluid were initially fixed at the same temperature, T'_∞. A transverse magnetic field that is perpendicular to the plate and has an intensity, B_0, that is constant, is meant to be applied. When the magnetic Reynolds number is low, the result of the induced magnetic field, which is significant, is irrelevant. The fluid is assumed to contain water-based magnetic nanoparticles such as aluminum oxide Al_2O_3 and cupper Cu. Figure 1 represents the physical model, Table 1 lists the thermophysical attributes of nanoparticles and thermal conductivity for spherical shaped nanoparticles are tabulated in Table 2.

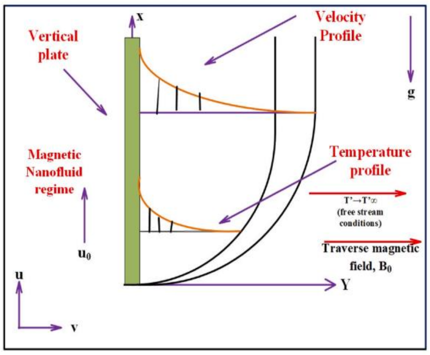

Figure 1. The physical model and coordinate system [29].

Table 1. Thermophysical properties of H_2O, Al_2O_3, and Cu.

	H_2O	Al_2O_3	Cu
$c_p\left(\mathrm{JKg^{-1}K^{-1}}\right)$	4179	765	8993
$\rho\left(\mathrm{Kgm^{-3}}\right)$	997.1	3970	385
$k\left(\mathrm{Wm^{-1}K^{-1}}\right)$	0.613	40	401
$\beta \times 10^{-5}\left(\mathrm{K^{-1}}\right)$	21	401	1.67

Cauchy tensor rheological state equation of Casson fluid [9] as follows:

$$\tau = \tau_0 + \mu\gamma'$$

$$\tau_{i,j} = \begin{Bmatrix} 2\left(\mu_B + \frac{P_y}{\sqrt{2\pi}}\right)e_{i,j}; & \pi > \pi_c \\ 2\left(\mu_B + \frac{P_y}{\sqrt{2\pi}}\right)e_{i,j}; & \pi < \pi_c \end{Bmatrix}$$

Here, μ_B is the dynamic viscosity plastic of Newtonian fluid, P_y is the fluid stress yield, $\pi = e_{i,j}e_{i,j}$ and $e_{i,j}$ are the components of the deformation rate, and π_c is critical value. This analysis is carried out under the following assumptions: the fluid is incompressible, non-Newtonian and the unconfined convection flow is unsteady and one-directional, the plate is rigid, and the vertical plate is oscillating, viscous dissipation terms in the energy equation are neglected. Then, the following set of governing equations and flow configuration of the problem are as follows:

Using the conventional Boussinesq approximation, the momentum, energy, and mass equations controlling the flow are as follows [29,33], taking into account the aforementioned assumptions:

$$\frac{\partial v^*}{\partial y^*} = 0 \tag{1}$$

$$\frac{\partial u^*}{\partial t^*} + v\frac{\partial u^*}{\partial y^*} = v_{nf}\left(1 + \frac{1}{\beta}\right)\frac{\partial^2 u^*}{\partial y^{*2}} - \frac{\sigma_{nf}}{\rho_{nf}}{B_0}^2 u^* + \frac{g(\rho\beta)_{nf}}{\rho_{nf}}(T^* - {T^*}_\infty) \tag{2}$$

$$\frac{\partial T^*}{\partial t^*} + v\frac{\partial T^*}{\partial y^*} = \frac{k_{nf}}{(\rho c_p)_{nf}}\frac{\partial^2 T^*}{\partial y^{*2}} - \frac{1}{(\rho c_p)_{nf}}\frac{\partial q_r}{\partial y^*} + \frac{Q_1}{(\rho c_p)_{nf}}(C^* - {C^*}_\infty) + \frac{\mu_{nf}}{(\rho c_p)_{nf}}\left(\frac{\partial u^*}{\partial y^*}\right)^2 + \frac{D_m K_{nf}}{(\rho c_p)_{nf} c_s}\frac{\partial^2 C^*}{\partial y^{*2}} \tag{3}$$

$$\frac{\partial C^*}{\partial t^*} + v\frac{\partial C^*}{\partial y^*} = D\frac{\partial^2 C^*}{\partial y^{*2}} - K^*(C^* - {C^*}_\infty) + D_T\frac{\partial^2 T^*}{\partial y} \tag{4}$$

The subjected initial and associated boundary flow region circumstances are

$$\left.\begin{array}{l} u^* = 0, \quad T^* = T^*_\infty, \quad C^* = C^*_\infty \text{ at } t^* = 0 \text{ for all } y^* \geq 0, \\ u^* = u_0, \quad T^* = T^*_w, \quad C^* = C^*_w \text{ at } t^* > 0,\ y^* = 0, \\ u^* \to 0, \quad T^* \to T^*_\infty, \quad C^* \to C^*_\infty, \quad t^* > 0 \text{ as } y^* \to \infty \end{array}\right\} \tag{5}$$

Table 2. Thermal conductivity for spherical shaped nanoparticles [34].

Model	Shape of Nanoparticles	Thermal Conductivity
I	Spherical	$k_{nf} = k_f\left(\frac{k_s+2k_f-2\varphi(k_f-k_s)}{k_s+2k_f+\varphi(k_f-k_s)}\right)$
II	Spherical	$k_{nf} = k_f\left(\frac{k_s+2k_f-2\varphi(k_f-k_s)}{k_s+2k_f+\varphi(k_f-k_s)}\right)$

Equation (1) gives

$$v^* = -v_0(v_0 > 0)$$

Here, suction velocity v_0 is thought to be constant, and the plate is indicated by the negative sign.

The important attributes of nanofluid are

$$\begin{array}{c} \mu_{nf} = \frac{\mu_f}{(1-\varphi)^{2.5}}, \quad \rho_{nf} = (1-\varphi)\,\rho_f + \varphi\,\rho_s \\ (\rho c_p)_{nf} = (1-\varphi)(\rho c_p)_f + \varphi(\rho c_p)_s \\ (\rho\beta)_{nf} = (1-\varphi)(\rho\beta)_f + \varphi(\rho\beta)_s \\ \sigma_{nf} = \sigma_f\left(1 + \frac{3(\sigma-1)\varphi}{(\sigma+2)-(\sigma-1)\varphi}\right), \quad \sigma = \frac{\sigma_s}{\sigma_f} \end{array} \tag{6}$$

The radiation heat flux is expressed as

$$q_r = -\frac{4\sigma^*}{3k^*}\frac{\partial T^{*4}}{\partial y} \tag{7}$$

The symbol T^{*4} is termed as a linear function, expanded using Taylor series regarding free-stream velocity.

The specification of T^{*4} is that the difference of temperature $(T^* - T^*_\infty)$ is sufficiently small, and we have

$$T^{*4} = T^{*\,4}_\infty + 3T^{*\,3}_\infty(T^* - T^*_\infty) + 6T^{*\,2}_\infty(T^* - T^*_\infty)^2 + \ldots \tag{8}$$

In Equation (8), omitting higher order terms, we obtain

$$T^{*4} = 4T^{*3}_\infty T^* - 3T^{*4}_\infty \tag{9}$$

Using Equations (7) and (9), Equation (2) is transformed as

$$\frac{\partial T^*}{\partial t^*} + v\frac{\partial T^*}{\partial y^*} = \frac{1}{(\rho c_p)_{nf}}\left(k_{nf} + \frac{16\sigma^* T^{*\,3}_\infty}{3k^*}\right)\frac{\partial^2 T^*}{\partial y^{*2}} + Q_1(C^* - C^*_\infty) + \mu_{nf}\left(\frac{\partial u^*}{\partial y^*}\right)^2 + \frac{D_m K_{nf}}{(\rho c_p)_{nf} c_s}\frac{\partial^2 C^*}{\partial y^{*2}} \tag{10}$$

3. Numerical Procedure

The non-dimensional quantifiers [27] are

$$\eta = y = \frac{u_0 y^*}{v_f},\ t = \frac{{u_0}^2 t^*}{v_f},\ U = \frac{u^*}{u_0},\ \theta = \frac{T^* - T^*_\infty}{T^*_w - T^*_\infty},\ \phi = \frac{C^* - C^*_\infty}{C^*_w - C^*_\infty},\ M^2 = \frac{\sigma_1 {B_0}^2 v_f}{\rho_f}, Nr = \frac{16\sigma^* T^{*3}_\infty}{3k_f k^*},$$
$$\Pr = \frac{\mu_f c_p}{k_f},\ Gr = \frac{g\beta_f v_f (T^*_w - T^*_\infty)}{{u_0}^3},\ Sc = \frac{v}{D},\ Q = \frac{Q_1 v_f (C^*_w - C^*_\infty)}{{u_0}^2 (T^*_w - T^*_\infty)}, Du = \frac{D_m K_T (C^*_w - C^*_\infty)}{v c_s \left(\rho c_p\right)_f (T^*_w - T^*_\infty)}$$
$$Ec = \frac{u_0^2}{\left(c_p\right)_f (T^*_w - T^*_\infty)},\quad K_r = \frac{K(C^*_w - C^*_\infty) v_f}{u_0^2}, Sr = \frac{D_T (T^*_w - T^*_\infty)}{v_f (C^*_w - C^*_\infty)},\ \lambda = -\frac{v}{u_0}$$

Equations of fluid flow have been rewritten as

$$\frac{\partial U}{\partial t} - \lambda \frac{\partial U}{\partial y} = a_1 \left(1 + \frac{1}{\beta}\right) \frac{\partial^2 U}{\partial y^2} - M a_3 U + Gr\, a_2\, \theta \tag{11}$$

$$\frac{\partial \theta}{\partial t} - \lambda \frac{\partial \theta}{\partial y} = a_4 \frac{\partial^2 \theta}{\partial y^2} + a_5 Ec \left(\frac{\partial U}{\partial y}\right)^2 + Q\phi + Du \frac{\partial^2 \phi}{\partial y^2} \tag{12}$$

$$\frac{\partial \phi}{\partial t} - \lambda \frac{\partial \phi}{\partial y} = \frac{1}{Sc} \frac{\partial^2 \phi}{\partial y^2} - K_r \phi + Sr \frac{\partial^2 \theta}{\partial y^2} \tag{13}$$

The initial values and related boundary conditions are

$$\left.\begin{array}{l} U = 0,\ \theta = 0,\ \phi = 0,\ \text{at } t = 0 \text{ for all } y \geq 0, \\ U = 1,\ \theta = 1,\ \phi = 1,\ \text{at } t > 0,\ y = 0, \\ U \to 0,\ \theta \to 0,\ \phi \to 0,\ \ t > 0 \text{ as } y \to \infty \end{array}\right\} \tag{14}$$

Equation (11) is expressed using the Galerkin equation as

$$\begin{array}{l} \int_{y_j}^{y_k} N^{(e)^T} \left[\ a_1 \left(1 + \frac{1}{\beta}\right) \frac{\partial^2 U}{\partial y^2} - \frac{\partial U}{\partial t} + \lambda \frac{\partial U}{\partial t} - a_3 U + R\right] dy \\ \text{where } \ R = Gr a_2 \theta \end{array} \tag{15}$$

The approximate piecewise linear solution is

$$\begin{array}{c} U^{(e)} = \left(N_j(y) U_j(t)\right) + \left(N_k(y) U_k(t)\right) \\ N_j \left(= \frac{y_k - y}{y_k - y_j}\right),\ N_k \left(= \frac{y - y_j}{y_k - y_j}\right) \end{array} \tag{16}$$

$$a_1 \left(1 + \frac{1}{\beta}\right) N^{(e)^T} \frac{\partial U^{(e)}}{\partial y}\Big]_{y_j}^{y_k} - \left\{ \int_{y_j}^{y_k} a_1 \left(1 + \frac{1}{\beta}\right) \frac{\partial N^{(e)^T}}{\partial y} \frac{\partial U^{(e)}}{\partial y} + N^{(e)^T} \left(\frac{\partial U^{(e)}}{\partial t} - \lambda \frac{\partial U^{(e)}}{\partial y} + a_3 M U^{(e)} - R\right) \right\} dy = 0$$

From Equation (16) we obtain, by neglecting first term

$$\left\{ \int_{y_j}^{y_k} a_1 \frac{\partial N^{(e)^T}}{\partial y} \frac{\partial U^{(e)}}{\partial y} + N^{(e)^T} \left(\frac{\partial U^{(e)}}{\partial t} - \lambda \frac{\partial U^{(e)}}{\partial y} + a_3 M U^{(e)} - R\right) \right\} dy = 0$$

$$\frac{1}{l^e} \begin{bmatrix} 1 & -1 \\ -1 & 1 \end{bmatrix} \begin{bmatrix} U_j \\ U_k \end{bmatrix} + \frac{l^e}{6} \begin{bmatrix} 2 & 1 \\ 1 & 2 \end{bmatrix} \begin{bmatrix} \dot{U_j} \\ \dot{U_k} \end{bmatrix} + \frac{a_3 M l^e}{6} \begin{bmatrix} 2 & 1 \\ 1 & 2 \end{bmatrix} \begin{bmatrix} U_j \\ U_k \end{bmatrix} - \frac{\lambda}{2} \begin{bmatrix} -1 & 1 \\ -1 & 1 \end{bmatrix} \begin{bmatrix} U_j \\ U_k \end{bmatrix} = R \frac{l^e}{2} \begin{bmatrix} 1 \\ 1 \end{bmatrix}$$

where $l^e = y_k - y_j = h$ and dot associates to the first derivative of t.

The element equations are

$$\frac{a_1 \left(1 + \frac{1}{\beta}\right)}{l^e} \begin{bmatrix} 1 & -1 & 0 \\ -1 & 2 & -1 \\ 0 & -1 & 1 \end{bmatrix} \begin{bmatrix} U_{i-1} \\ U_i \\ U_{i+1} \end{bmatrix} + \frac{l^e}{6} \begin{bmatrix} 2 & 1 & 0 \\ 1 & 4 & 1 \\ 0 & 1 & 2 \end{bmatrix} \begin{bmatrix} \dot{U}_{i-1} \\ \dot{U}_i \\ \dot{U}_{i+1} \end{bmatrix} + a_3 \frac{M l^e}{6} \begin{bmatrix} 2 & 1 & 0 \\ 1 & 4 & 1 \\ 0 & 1 & 2 \end{bmatrix} \begin{bmatrix} U_{i-1} \\ U_i \\ U_{i+1} \end{bmatrix} - \frac{\lambda}{2} \begin{bmatrix} -1 & 1 & 0 \\ -1 & 0 & 1 \\ 0 & -1 & 1 \end{bmatrix} \begin{bmatrix} U_{i-1} \\ U_i \\ U_{i+1} \end{bmatrix} = R \frac{l^e}{2} \begin{bmatrix} 1 \\ 2 \\ 1 \end{bmatrix} \tag{17}$$

In Equation (17), the row corresponding to node i is equated to zero to obtain b

$$\frac{a_1 \left(1 + \frac{1}{\beta}\right)}{{l^{(\mathbf{e})}}^2} [-U_{i-1} + 2U_i + U_{i+1}] + \frac{1}{6} \left[\dot{U}_{i-1} + 4\dot{U}_i + \dot{U}_{i+1}\right] + a_3 \frac{M}{6} [U_{i-1} + 4U_i + U_{i+1}] - \frac{\lambda}{2l^e} [-U_{i-1} + U_{i+1}] = R$$

To the above equation, utilizing the Crank–Nicholson method, we obtain

$$A_1U_{i-1}^{j+1} + A_2U_i^{j+1} + A_3U_{i+1}^{j+1} = A_4U_{i-1}^{j} + A_5U_i^{j} + A_6U_{i+1}^{j} + R^* \tag{18}$$

$$B_1\theta_{i-1}^{j+1} + B_2\theta_i^{j+1} + B_3\theta_{i+1}^{j+1} = B_4\theta_{i-1}^{j} + B_5\theta_i^{j} + B_6\theta_{i+1}^{j} + Q^* \tag{19}$$

$$D_1\phi_{i-1}^{j+1} + D_2\phi_i^{j+1} + D_3\phi_{i+1}^{j+1} = D_4\phi_{i-1}^{j} + D_5\phi_i^{j} + D_6\phi_{i+1}^{j} + P^* \tag{20}$$

$$A_1 = 2 - 6a_1\left(1+\tfrac{1}{\beta}\right)r + M*k + (3\lambda rh),\ \ A_2 = 8 + 12a_1\left(1+\tfrac{1}{\beta}\right)r + 4M*k\,,$$
$$A_3 = 2 - 6a_1\left(1+\tfrac{1}{\beta}\right)r + M*k - (3\lambda rh),\ \ A_4 = 2 + 6a_1\left(1+\tfrac{1}{\beta}\right)r - M*k - (3\lambda rh),$$
$$A_5 = 8 - 12a_1\left(1+\frac{1}{\beta}\right)r - 4M*k, \quad A_6 = 2 + 6a_1\left(1+\frac{1}{\beta}\right)r - M*k + (3\lambda rh)$$
$$R^* = 12(kGrT_i)$$

The values of a_i are given in Appendix A.

Applying analogous method to Equations (8), (9), and (12), we obtain

$$B_1 = 2 - 6a_4*r + (3\lambda rh)*\mathrm{Pr}, \quad B_2 = 8 + 12*r + k, \quad B_3 = 2 - 6*r + k - (3\lambda rh)*\mathrm{Pr},$$

$$B_4 = 2 + 6a_4*r - (3\lambda rh)*\mathrm{Pr}, \quad B_5 = 8 - 12a_4*r, \quad B_6 = 2 + 6a_4*r + (3\lambda rh)*\mathrm{Pr},$$

$$Q^* = 12kEca_5\mathrm{Pr}\left(\frac{\partial u_i}{\partial y}\right)^2 + 12k\mathrm{Pr}QC_i + Dua_5\frac{\partial^2 C_i}{\partial y^2},$$

$$D_1 = (2Sc) - (6r) + \delta Sck + (3\lambda rh)*Sc,\ \ D_2 = (8Sc) + (12r) + 4\delta Sck,\ D_3 = (2Sc) - (6r) + \delta Sck - (3\lambda rh)*Sc,$$
$$D_4 = (2Sc) + (6r) - \delta Sck - (3\lambda rh)*Sc,\ \ D_5 = (8Sc) - (12r) - 4\delta Sck,\ D_6 = (2Sc) + (6r) - \delta Sck + (3\lambda rh)*Sc,$$
$$P^* = So\tfrac{\partial^2 T_i}{\partial y^2}$$

$r = \frac{k}{h^2}$, h, k are the sizes of mesh points connected to the direction of y and parameter of time t. In Equations (15)–(18), taking i = 1 to n and using initial and boundary conditions (Equation (11)), the following system of equations in the matrix notation are obtained:

$$A_iX_i = B_i\ i = 1, 2,\ 3 \tag{21}$$

The solutions of the above equations, obtained by employing Galerkin FEM, lead to stable and convergent numerical results, presented graphically using MATLAB Software.

4. Findings and Discussion

In order to determine the problem's physical significance, mathematical forecasts of concentration, temperature, and velocity have been made for a variety of guesses of suitable non-dimensional flow parameters. The effect of the heat source, Dufour effect, and viscous dissipation on Nusselt number are illustrated in Table 3. It is evident that the Nusselt number drops with heat generation and the Eckert number, whereas it elevates with the Dufour number. The distribution of skin friction and the Nusselt number for the Cu–water nanofluid are listed in Table 4. The skin-friction coefficient is observed to decrease with increasing values of M and λ, but to increase with increasing estimates of Gr and R. Additionally, it is found that Nusselt number values drop as M and R values rise.

Table 3. The Nusselt number $Nu = -\frac{K_{nf}}{K_f}\left(\frac{\partial\theta}{\partial y}\right)_{y=0}$, Pr = 7.

Q	Du	Ec	Nu
0.2	0.5	0.01	0.5765
0.5			0.2624
1.0			−0.4015
	1.0		0.5721
	1.5		0.5701
		0.02	0.5677
		0.03	0.5601

Table 4. Numerical values of Skin friction (C_f) and Nusselt number ($\theta'(0)$) with Pr = 6.2, φ = 0.05 and Ec = 0.01 for Cu-water nanofluid as $\beta \to \infty$.

Gr	M	λ	R	Present		Previous (Khan et al. [27])	
				C_f	$-\theta'(0)$	C_f	$-\theta'(0)$
5	1	0.2	1	0.7295	1.1654	0.7296	1.1653
10				2.6396		2.6395	
	3			−0.2742	1.0512	−0.2741	1.0511
	5			−0.9281	1.0488	−0.9283	1.0488
		0.3		0.586		0.5867	
		0.4		0.4377		0.4378	
			2	1.0480	0.7974	1.0479	0.7973
			3	1.2629	0.6620	1.2629	1.2630

The fluid velocity uplift as the Gr increases is shown in Figure 2. The Gr is the ratio of buoyancy force to viscous force. When Gr < 1, the viscous force takes over the buoyancy and causes an uptick in the nanofluid, which causes increased movement. The effect of the magnetic field on the velocity profile of the Cu nanofluid is depicted in Figure 3. The fluid flow is opposed by the Lorenz force, which is produced by the existence of a magnetic field. This force's amplitude is directly proportional to the magnitude of M. Therefore, the Lorentz force is strengthened as M increases. Thus, the momentum is observed to diminish with higher values of M. This, in turn, increases the fluid flow's resistance.

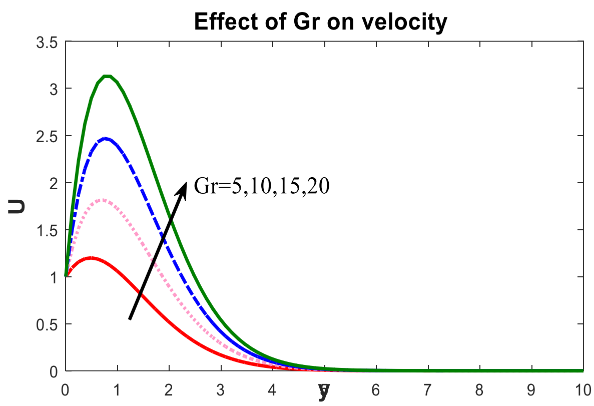

Figure 2. Effect of Gr on velocity.

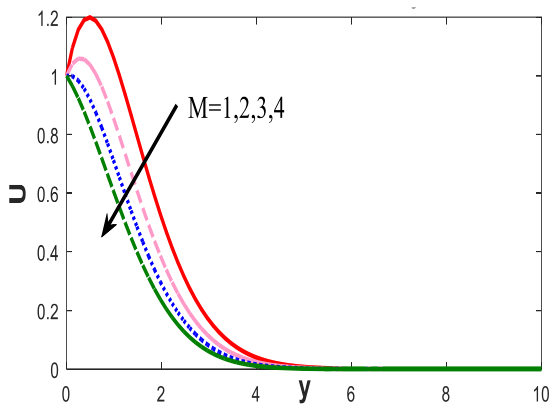

Figure 3. Effect of M on velocity.

The consequence of viscous dissipation on velocity and temperature is demonstrated in Figures 4 and 5. Due to the relationship between kinetic energy and enthalpy difference, velocity and temperature are boosted when Ec increases.

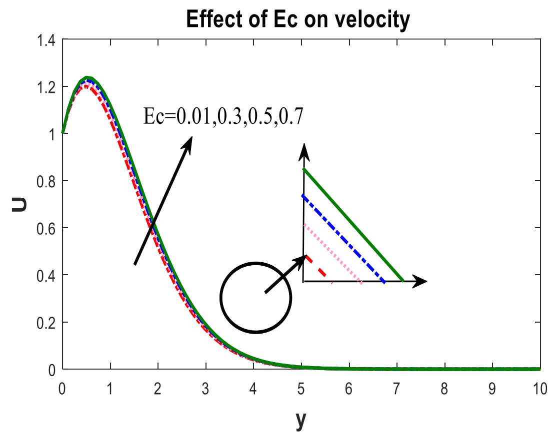

Figure 4. Effect of Ec velocity.

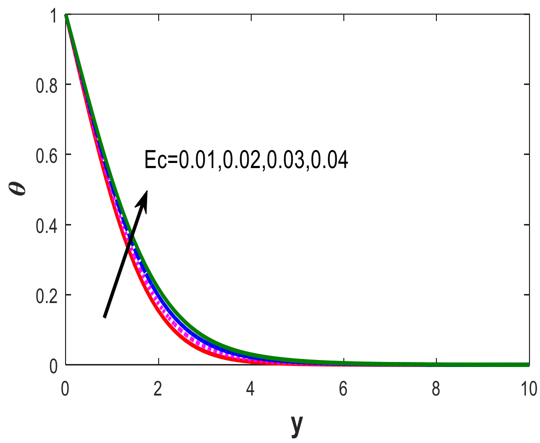

Figure 5. Effect of Ec on temperature.

Heat and mass are more effectively transmitted as a result of Soret and Dufour impressions. Figures 6 and 7 are shown to demonstrate the Dufour effect on velocity and temperature. The ratio of concentration difference to temperature is called Soret. It is perceived that velocity and temperature are boosted with growing values of Dufour and, hence, heat transfer escalates. Figures 8–10 present the impact of Soret on velocity, temperature, and concentration. The velocity and temperature of the fluid decrease as Sr increases, while mass transfer accelerates.

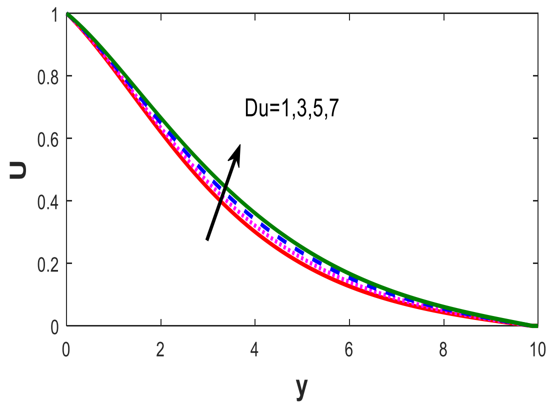

Figure 6. Effect of Du on velocity.

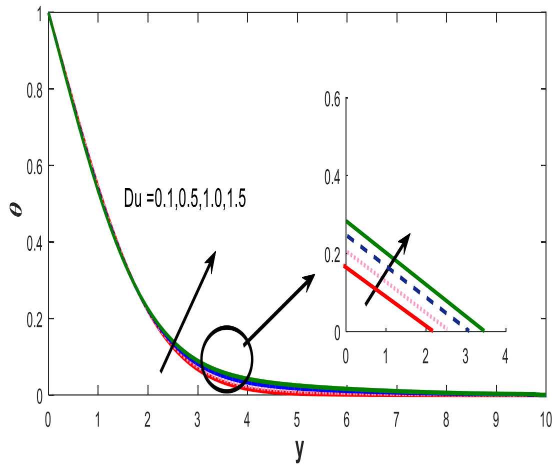

Figure 7. Effect of Du on temperature.

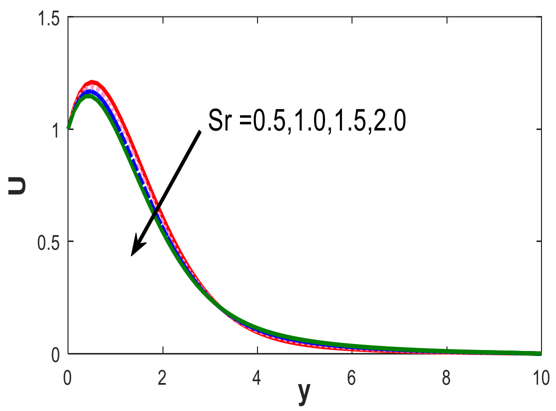

Figure 8. Effect of Sr on velocity.

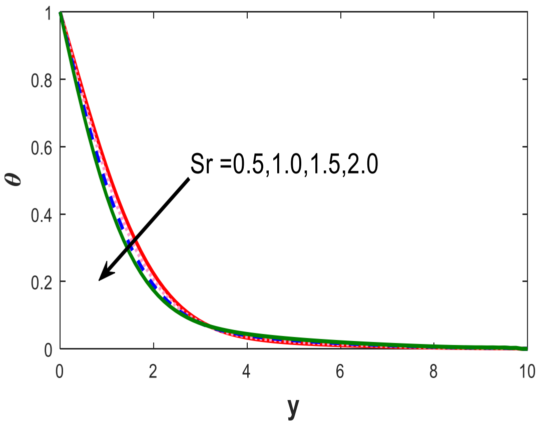

Figure 9. Effect of Sr on temperature.

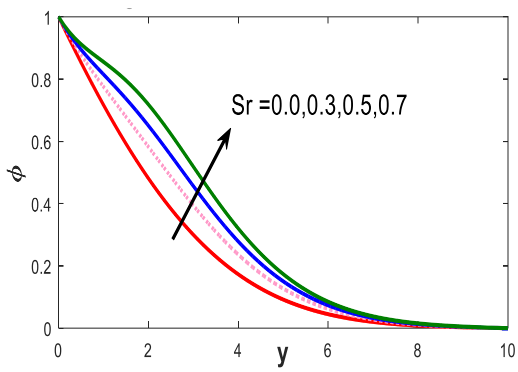

Figure 10. Effect of Sr on concentration.

Figures 11 and 12 are illustrated to demonstrate the variation of heat source and sink on fluid velocity and temperature. It is evident from the profiles that the thermal conductivity increases with the enhancement of the heat source (Q); this is because of enrichment in the thermal boundary layer thickness. Physically, dominant values of the Q contribute more heat to the working fluid, causing the thermal profile to accelerate. Hence, the velocity and temperature of the fluid are boosted. Figures 13 and 14 depict the effects of radiation on velocity and temperature. The random movement of nanoparticles is enhanced by the addition of R to the temperature field. Therefore, the constant collision causes additional heat to be produced. Consequently, a rise in temperature and velocity is noted. Changes in fluid concentration due to the chemical reaction parameter K are displayed in Figure 15. It explains that as the value of Kr increases, the concentration of nanoparticles decreases.

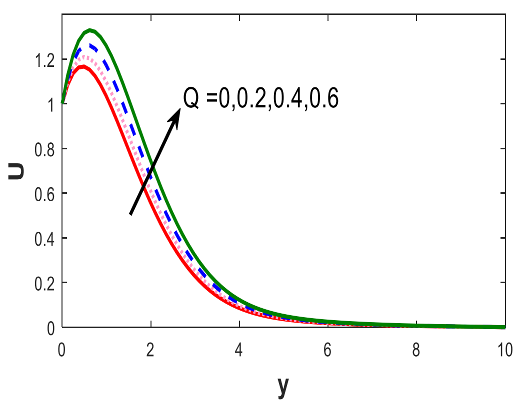

Figure 11. Effect of Q on velocity.

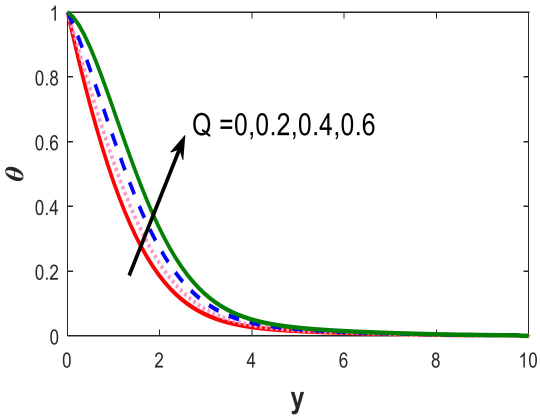

Figure 12. Effect of Q on temperature.

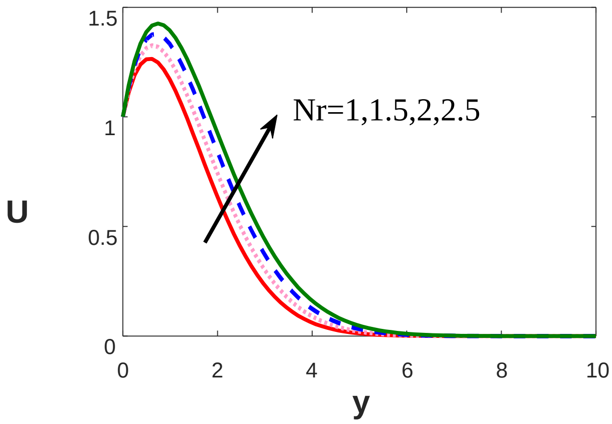

Figure 13. Effect of Nr on velocity.

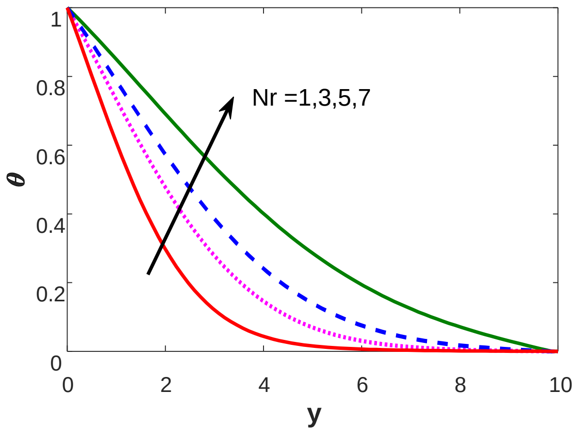

Figure 14. Effect of Nr on temperature.

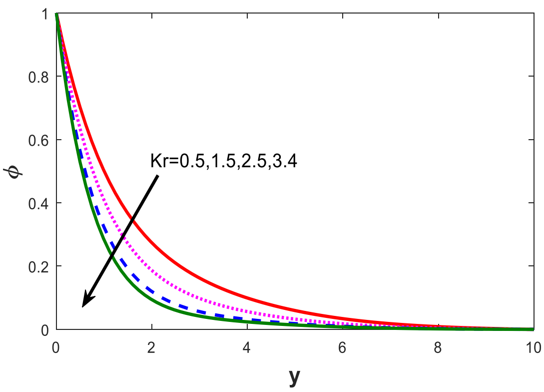

Figure 15. Effect of Kr on concentration.

Figure 16 explains the influence of the Schmidt number on concentration. As we know, the Schmidt number is the ratio of kinematic viscosity and mass diffusivity. Due to the enhancement of the Schmidt number, mass diffusivity dominates the kinematic viscosity, which leads to a depreciation of the concentration. Volume fraction effects on temperature are observed in Figure 17. The interaction between particles in base fluids, which is brought on by the random movement of particles, increases as the volume fraction of nanoparticles in the fluid increases.

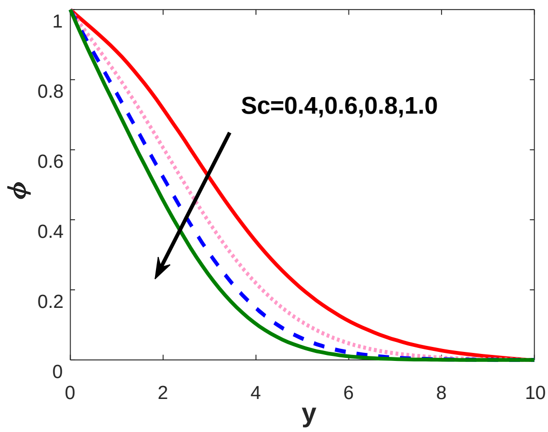

Figure 16. Effect of SC on concentration.

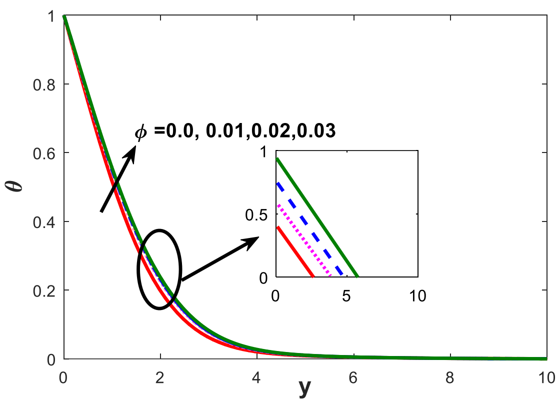

Figure 17. Effect of ϕ on temperature.

Figure 18a,b show a comparison of the effects of fluid and (Cu-water-based) nanofluid on velocity and temperature. It is clear from the profiles that the velocity decreases and the temperature of the nanofluid is higher than that of the Casson fluid. Compared to Casson fluid, thermal boundary thickness is increased in Casson nanofluid due to the temperature distribution being higher and the velocity profile being lower.

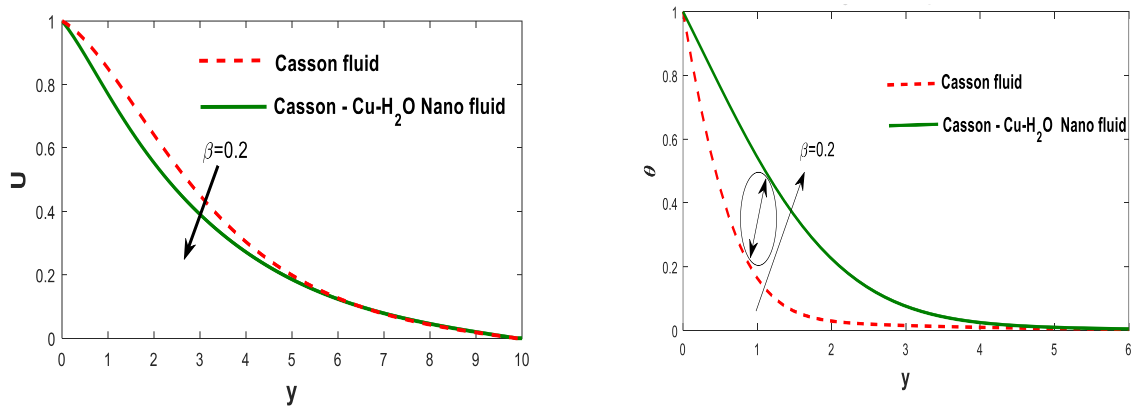

Figure 18. Comparisons of Casson fluid with Casson nanofluid (**a**) Velocity (**b**) Temperature.

In Figure 19a,b, the Casson parameter's influence on the velocity and temperature profiles is presented. As a result, as the Casson parameter increases and the nanofluid flow decelerates away from the surface, resulting in a smaller boundary layer. Temperature distributions are greater in the event of a large Casson parameter than in the case of a small Casson value.

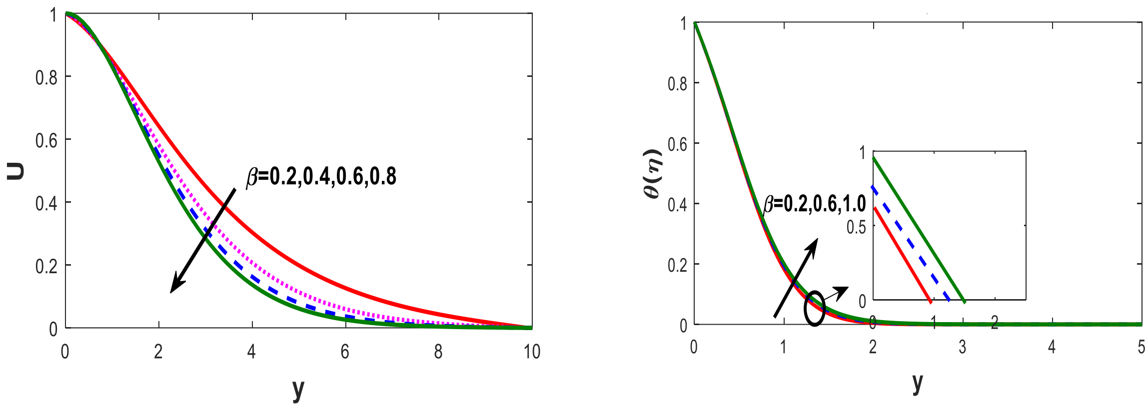

Figure 19. (**a**) Effect of β on velocity; (**b**) Effect of β on temperature.

The impact of the Dufour effect on the Nusselt number Nu for distinct values of nanoparticle volume fraction φ is portrayed in Figures 20 and 21. It can be understood from the figures that the heat transfer gradually increases with Du while it comes down with the rise in Q, while Nu is constant with Sr for different values of Radiation parameter, as noted in Figure 22. According to Figure 23, skin friction gradually decreases as Gr increases.

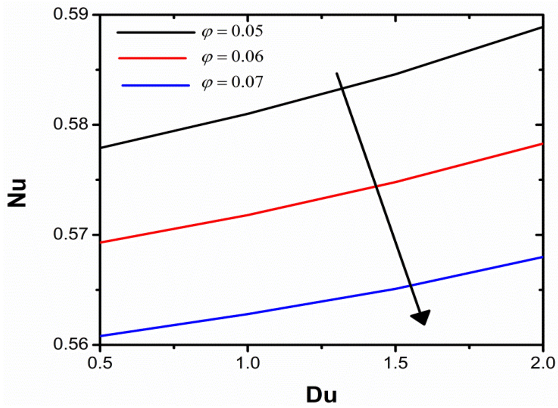

Figure 20. Variation of Nu vs. Du with φ.

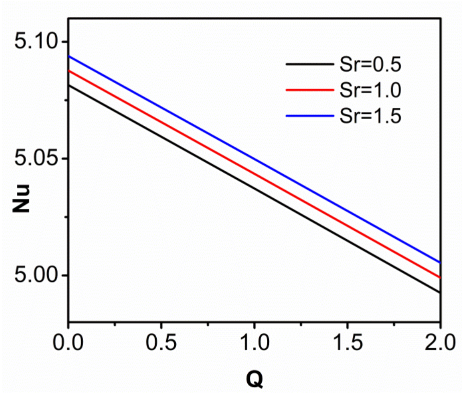

Figure 21. Variation of Nu vs. Q with Sr.

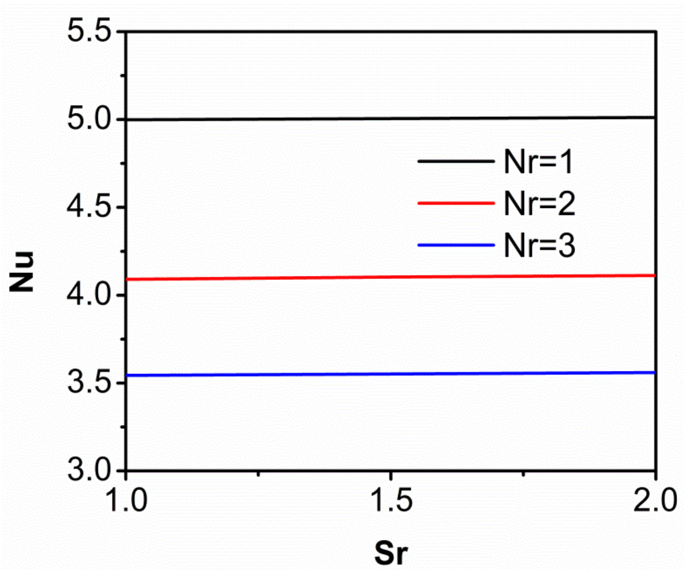

Figure 22. Variation of Nu vs. Sr with Nr.

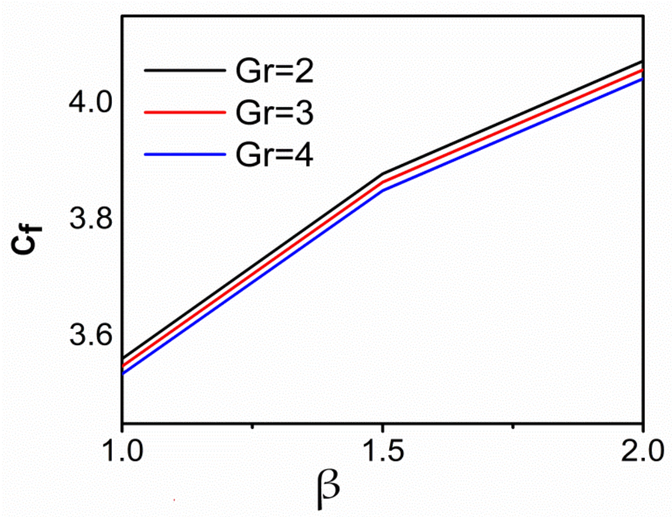

Figure 23. Variation of C_f vs. β with Gr.

5. Conclusions

This paper examined the transient MHD free-convection flow and heat transfer of a nanofluid past a vertical plate in the presence of Soret and Dufour effects. Numerical calculations are carried out for various values of the dimensionless parameters. The effects of different physical parameters on the mass, heat, and flow characteristics of nanofluids were investigated.

- ➢ Fluid velocity rises with the Grashof number while it falls in the magnetic field.
- ➢ The effects of Prandtl number and viscous dissipation are to improve the velocity and temperature.
- ➢ The Dufour effect raises the velocity and temperature while reducing due to the Soret effect.
- ➢ Thermal conductivity is enhanced by heat sources and radiation.
- ➢ With chemical reaction and Schmidt number, concentration decreases.
- ➢ Rate of heat transfer accelerated with Du values and retards with the values of Q and Ec.

Author Contributions: Conceptualization, methodogy, software, R.K. and B.S.R.; validation, formal analysis, investigation, R.K., B.S.R. and C.C.; resources, data curation, writing-original draft preparation, R.K., B.S.R. and H.S.N.; writing-review and editing, B.S.R. and C.C.; visualization, R.K. and C.C.; supervision, project administration, funding acquisition, R.K. and B.S.R. All authors have read and agreed to the published version of the manuscript.

Funding: This research received no external funding.

Data Availability Statement: Not applicable.

Acknowledgments: The authors thank the reviewers and the editorial team for their constructive comments in improving the quality of the article.

Conflicts of Interest: The authors declare no conflict of interest.

Nomenclature

B_0	Applied magnetic field
C	Non-dimensional concentration
C_p	Specific heat (constant pressure)
C^*	Species concentration
$C_\infty{}^*$	Free stream concentration
$C_w{}^*$	Species concentration at wall
Du	Dufour number
g	Acceleration due to gravity
Gr	Grashof number
K	Permeability parameter
k_f	Thermal conductivity of the base fluid
k_s	Thermal conductivity of the nanoparticles
k_{nf}	Thermal conductivity of the nanofluid
k^*	Mean absorption coefficient
M	Magnetic field parameter
N_r	Radiation parameter
Pr	Prandtl number
Q	Heat generation parameter
T	Non-dimensional temperature
T^*	Temperature
$T_\infty{}^*$	Free-stream temperature
t^*	Time
$T_w{}^*$	Temperature at wall
Sc	Schmidt number
Sr	Soret number
φ	Solid volume fraction of the nanoparticle
δ	Chemical reaction parameter
λ	Buoyancy parameter
u^*	Velocity components along $x^*{-}y^*$ direction
u_0	Initial velocity
nf	Nanofluid
q_r	Radiative heat flux
σ_{nf}	Electrical conductivity of the nanofluid
β_{nf}	Thermal expansion coefficient of the nanofluid
(x^*, y^*)	Dimensional co-ordinates
ρ_{nf}	Nanofluid density
μ_f	Viscosity of the base fluid

Appendix A

$$a_1 = \frac{1}{(1-\varphi)^{2.5}\left((1-\varphi)+\varphi\frac{(\rho s)}{(\rho p)}\right)}, \quad a_2 = \frac{\left((1-\varphi)+\varphi\frac{(\rho\beta)_s}{(\rho\beta)_f}\right)}{\left((1-\varphi)+\varphi\frac{(\rho s)}{(\rho p)}\right)}, \quad a_3 = \frac{1}{\left((1-\varphi)+\varphi\frac{(\rho s)}{(\rho p)}\right)},$$

$$a_4 = \frac{K_f\left(\frac{k_s+2k_f-2\varphi\left(k_f-k_s\right)}{k_s+2k_f+\varphi\left(k_f-k_s\right)}\right)+Nr}{\left((1-\varphi)+\varphi\frac{(\rho c p)_s}{(\rho c p)_f}\right)}, \quad a_5 = \frac{1}{(1-\varphi)^{2.5}\left((1-\varphi)+\varphi\frac{(\rho c p)_s}{(\rho c p)_f}\right)}$$

References

1. Choi, S.U.; Eastman, J.A. Enhancing thermal conductivity of fluids with nanoparticles. *ASME-Publ. Fed* **1995**, *231*, 99–106.
2. Upreti, H.; Pandey, A.K.; Kumar, M. MHD flow of Ag-water nanofluid over a flat porous plate with viscous-ohmic dissipation, suction/injection and heat generation/absorption. *Alexander Eng. J.* **2018**, *57*, 1839–1847. [CrossRef]
3. Mishra, A.; Pandey, A.K.; Chamkha, A.J.; Kumar, M. Roles of nanoparticles and heat generation/absorption on MHD flow of Ag-H_2O nanofluid via porous stretching/shrinking convergent/divergent channel. *J. Egypt Math. Soc.* **2020**, *28*, 17. [CrossRef]

4. Ibrahim, W.; Negera, M. MHD slip flow of upper convected Maxwell nanofluid over stretching sheet with chemical reaction. *J. Egypt. Math. Soc.* **2020**, *28*, 7. [CrossRef]
5. Kataria, H.R.; Patel, H.R. Effect of chemical reaction and heat generation/absorption on Magneto hydrodynamic(MHD) Casson fluid flow over an exponentially accelerated vertical plate embedded in porous medium with ramped wall temperature and ramped surface concentration. *Propuls. Power Res.* **2018**, *8*, 35–46. [CrossRef]
6. Kumar, M.S.; Sandeep, N.; Kumar, B.R. A comparative study of chemically reacting 2D flow of Casson and Maxwell fluids. *Alex. Eng. J.* **2017**, *57*, 2027–2034. [CrossRef]
7. Swain, B.K.; Parida, B.C.; Kar, S.; Senapati, N. Viscous dissipation and joule heating effect on MHD flow and heat transfer past a stretching sheet embedded in a porous. *Heliyon* **2020**, *6*, e05338. [CrossRef]
8. Muhammad, T.; Alishehzad, S.; Alsaedi, A. Viscous dissipation and Joule heating effects in MHD 3D flow with heat and mass fluxes. *Results Phys.* **2018**, *8*, 365–371. [CrossRef]
9. Reddy, G.J.; Srinivasa Raju, R.; Anand Rao, J. Influence of viscous dissipation on unsteady MHD natural convective flow of Casson fluid over an oscillating vertical plate via FEM. *Ain Shams Eng. J.* **2018**, *4*, 1907–1915. [CrossRef]
10. Jha, B.; Aina, B. Impact of induced magnetic field on MHD natural convection flow in a vertical annular micro channel in the presence of Radial magnetic field. *Propuls. Power Res.* **2018**, *7*, 171–181. [CrossRef]
11. Zainal, N.A.; Nazar, R.; Naganthran, K.; Pop, I. Heat generation/absorption effect on MHD flow of hybrid nanofluid over bidirectional exponential stretching/shrinking sheet. *Chin. J. Phys.* **2020**, *69*, 118–133. [CrossRef]
12. Raza, J.; Rohni, A.M.; Omar, Z. MHD flow and heat transfer of Cu–water nanofluid in a semi porous channel with stretching walls. *Int. J. Heat Mass Transf.* **2016**, *103*, 336–340. [CrossRef]
13. Soumya, D.O.; Gireesha, B.J.; Venkatesh, P. Planar Coquette flow of power law nanofluid with chemical reaction nano particle injection and variable thermal conductivity. *Sage Publ.* **2022**, *236*, 5257–5268.
14. Sarafraz, M.M.; Pourmehran, O.; Yang, B.; Arjomandi, M.; Ellahi, R. Pool boiling heat transfer characteristics of iron oxide nano-suspension under constant magnetic field. *Int. J. Therm. Sci.* **2020**, *147*, 106131. [CrossRef]
15. Majeed, A.; Zeeshan, A.; Bhatti, M.M.; Ellahi, R. Heat transfer in magnetite (Fe_3O_4) nanoparticles suspended in conventional fluids: Refrigerant-134A (C2H2F4), kerosene (C10H22), and water (H2O) under the impact of dipole. *Heat Transf. Res.* **2020**, *51*, 217–232. [CrossRef]
16. Mishra, A.; Pandey, A.K.; Kumar, M. Velocity, thermal and concentration slip effects on MHD silver-water nanofluid past a permeable cone with suction/injection and viscous-Ohmic dissipation. *Heat Transf. Res.* **2019**, *50*, 1351–1367. [CrossRef]
17. Megahed, A.M. Flow and heat transfer of non-Newtonian Sisko fluid past a nonlinearly stretching sheet with heat generation and viscous dissipation. *J. Braz. Soc. Mech. Sci. Eng.* **2018**, *40*, 492. [CrossRef]
18. Elbashbeshy, M.A.R.; Abdelgaber, K.; Asker, H.G. Heat and mass transfer of a Maxwell nanofluid over a stretching surface with variable thickness embedded in porous medium. *Int. J. Math. Comput. Sci.* **2018**, *4*, 86–98.
19. Hayat, T.; Ullah, I.; Muhammad, T.; Alsaedi, A. Radiative three-dimensional flow with Soret and Dufour effects. *Int. J. Mech. Sci.* **2017**, *133*, 829–837. [CrossRef]
20. Saritha, K.; Rajasekhar, M.; Reddy, B. Combined effects of Soret and Dufour on MHD flow of a power-law fluid over flat plate in slip flow Rigime. *Int. J. Appl. Mech. Eng.* **2018**, *23*, 689–705. [CrossRef]
21. Reddy, B.S.; Saritha, K. MHD Boundary Layer Slip Flow over a Flat Plate with Soret and Dufour effects. *Appl. Appl. Math. Int. J. (AAM)* **2019**, *14*, 31–43.
22. Pattnaik, J.R.; Dash, G.C.; Singh, S. Radiation and mass transfer effects on MHD flow through porous medium past an exponentially accelerated inclined plate with variable temperature. *Ain Shams Eng. J.* **2017**, *8*, 67–75. [CrossRef]
23. Sheikholeslami, M.; GorjiBandpy, M.; Ellahi, R.; Hassan, M.; Soleimani, S. Effects of MHD on Cu-water nanofluid flow and heat transfer by means of CVFEM. *J. Magn. Magn. Mater.* **2014**, *349*, 188–200. [CrossRef]
24. Rashidi, M.; Ganesh, N.V.; Hakeem, A.A.; Ganga, B. Buoyancy effect on MHD flow of nanofluid over a stretching sheet in the presence of thermal radiation. *J. Mol. Liquids* **2014**, *198*, 234–238. [CrossRef]
25. Madhu, M.; Kishan, N.; Chamkha, A.J. MHD flow of a non-Newtonian nanofluid over a nonlinearly stretching sheet in the presence of thermal radiation with heat source/sink. *Eng. Comput.* **2016**, *33*, 1610–1626. [CrossRef]
26. Khan, U.; Zaib, A.; Ishak, A. Magnetic field effect on Sisko fluid flow containing gold nanoparticles through a porous curved surface in the presence of radiation and partial slip. *Mathematics* **2021**, *9*, 921. [CrossRef]
27. Khan, U.; Zaib, A.; Abu Bakar, S.; Ishak, A. Stagnation-point flow of a hybrid nanoliquid over a non-isothermal stretching/shrinking sheet with characteristics of inertial and microstructure. *Case Stud. Therm. Eng.* **2021**, *26*, 101150. [CrossRef]
28. Parasuraman, L.; Krishnamurthy, D. Prandtl boundary layer flow of a Casson nanofluid past a permeable vertical plate. *Acta Tech. Corviniensis-Bull. Eng.* **2019**, *12*, 95–100.
29. Kumar, M.A.; Reddy, Y.D.; Rao, V.S.; Goud, B.S. Thermal radiation impact on MHD heat transfer natural convective nano fluid flow over an impulsive started vertical plate. *Case Stud. Therm. Eng.* **2020**, *24*, 100826. [CrossRef]
30. Chang, H.; Jwo, C.S.; Lo, C.H.; Tsung, T.T.; Kao, M.J.; Lin, H.M. Rheology of CuO Nanoparticle suspension prepared by ASNSS. *Rev. Adv. Mater. Sci.* **2005**, *10*, 128–132.
31. Rajesh, V.; Mallesh, M.P.; Beg, O.A. Transient MHD free convection flow and heat transfer of nanofluid past an impulsively started vertical porous plate in the presence of viscous dissipation. *Procedia Mater. Sci.* **2015**, *10*, 80–89. [CrossRef]

32. Tiwari, R.K.; Das, M.K. Heat transfer augmentation in a two-sided lid-driven differentially heated square cavity utilizing nanofluids. *Int. J. Heat Mass Transf.* **2007**, *50*, 2002–2018. [CrossRef]
33. Bejawada, S.G.; Yanala, D.R. Finite element Soret Dufour effects on an unsteady MHD heat and mass transfer flow past an accelerated inclined vertical plate. *Heat Transf.* **2021**, *50*, 8553–8578. [CrossRef]
34. Maxwell, J.C. *A Treatise on Electricity and Magnetism*; Clarendon Press: London, UK, 1881; Volume 1.